High Pressure Intrusion–Extrusion of LiCl Aqueous Solutions in Silicalite-1 Zeolite: Influence on Energetic Performances

ARTICLE *in* THE JOURNAL OF PHYSICAL CHEMISTRY C · FEBRUARY 2014

Impact Factor: 4.77 · DOI: 10.1021/jp4105163

6 AUTHORS, INCLUDING:

Ismail Khay
Université de Haute-Alsace
8 PUBLICATIONS **22** CITATIONS

SEE PROFILE

T. Jean Daou
Université de Haute-Alsace
68 PUBLICATIONS **1,197** CITATIONS

SEE PROFILE

Séverinne Rigolet
Institut de Science des Matériaux de Mulhouse
85 PUBLICATIONS **765** CITATIONS

SEE PROFILE

THE JOURNAL OF PHYSICAL CHEMISTRY C

Article

pubs.acs.org/JPCC

High Pressure Intrusion−Extrusion of LiCl Aqueous Solutions in Silicalite-1 Zeolite: Influence on Energetic Performances

I. Khay, T. J. Daou,* H. Nouali, A. Ryzhikov, S. Rigolet, and J. Patarin*

Equipe Matériaux à Porosité Contrôlée (MPC), Institut de Science des Matériaux de Mulhouse (IS2M), Université de Haute Alsace (UHA), CNRS, UMR 7361, ENSCMu, 3 bis rue Alfred Werner, F-68093 Mulhouse, France

ABSTRACT: The energetic performances of different "Silicalite-1−LiCl aqueous solution" systems were evaluated under high pressure. Depending on the LiCl concentration in the aqueous medium (0 M, 5 M, 10 M, 20 M), an increase of the intrusion and extrusion pressures and therefore of the stored (~10, ~13, ~19, ~31 J/g) and restored (~10, ~13, ~18, ~27 J/g) energies are observed. Thus, compared to the "Silicalite-1−water" system, the stored energy is tripled in the case of "Silicalite-1−LiCl 20 M" system. Several characterizations (XRD, TG, NMR, N_2 physisorption, ICP/OES, ...) have been realized before and after intrusion−extrusion experiments in order to reveal the presence or the lack of defects and the possible presence of lithium ions in the material after such experiments. At the short-range order, solid state NMR spectroscopy get evidence of the presence of Q_2 and Q_3 groups revealing the breaking of some siloxane bridges after the intrusion-extrusion steps and thus the creation of hydroxyl groups set in evidence by TG experiments. Only few traces of lithium (1 atom per unit cell) were found by ICP/OES analysis.

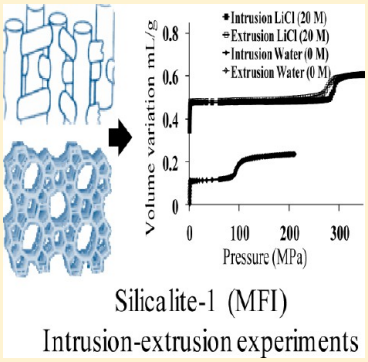

1. INTRODUCTION

The environmentally friendly and economically beneficial applications of zeolites in industrial catalysis, adsorption, and ion-exchange processes are well-known.[1,2] This success drives a continuing effort into the research of other potential applications of the zeolites. In this regards, the thermodynamics of confined systems involving water as nonwetting liquid and hydrophobic microporous solids such as purely silica zeolites (zeosils) have attracted considerable attention due to their potential application in the energetic field.[3] Since our pioneering work in 2001[3], several "zeosil−water" systems have already been studied[4−12] and a summary of the energetic performances of these zeosils is reported in our previous paper.[10] The "hydrophobic zeolites−water" systems showed different behaviors, depending on various physical parameters related to the porous matrix such as pore size, pore system (cages or channels), dimensionality of the channels and on the hydrophobic/hydrophilic character. According to the reversible or irreversible character of the intrusion−extrusion cycle, the "zeosils-water" systems are able to restore, absorb or dissipate mechanical energy. Consequently, molecular spring, bumper or shock-absorber behavior can be observed.

This process was recently also extended to another family of hydrophobic microporous materials, the metal organic framework materials (MOFs) such as ZIF-8 which displays a shock absorber behavior at a quite low pressure (27 MPa).[13]

Among hydrophobic zeolites, the most studied solid was the MFI-type zeosil (Silicalite-1); a pure-silica zeolite characterized by a three-dimensional channel system with 10-membered ring (MR) openings (0.55−0.56 nm). The "Silicalite-1−water" system acts as a molecular spring. It is able to restore 94% of the stored energy and this after three water intrusion−extrusion cycles. However, the stored energy close to 10−11 J/g of zeolite is quite low.[10]

In order to increase the stored energy, a first approach was to increase the pore volume with materials more porous than zeolites such as grafted mesoporous materials.[14−17] Another way to increase the stored energy can be achieved by increasing the intrusion pressure. This aim can be reached by replacing pure water with aqueous electrolyte solutions, the solid−liquid interfacial tension being usually higher compared to pure water.[18] Recently, the influence of the intrusion of saturated electrolytes like $MgCl_2$, NaCl, and LiCl solution in purely silica zeolite "Silicalite-1" on its energetic performances has been studied in our group.[19] The addition of salts into the "Silicalite-1−water" system strongly increases the energetic performances. The stored energy was found to be higher in the case of "Silicalite-1−LiCl·3H_2O" system due to the higher solubility (concentration) of the LiCl salt in water compared to $MgCl_2$ and NaCl and to the smallest size of the lithium cation compared to the sodium and magnesium cations.[19] A. Han et al. observed the same impact of ion size on the intrusion pressure and hence the stored energy in the cases of MCM-41 mesoporous material[20] and dealuminated zeolite Y,[21] intruded with aqueous solution of LiCl, NaCl, KCl, or CsCl and NaF, NaCl, or NaBr, respectively.

In this work, we present the influence of the LiCl electrolyte concentration on the energetic performances of MFI-type zeosil (Silicalite-1) using intrusion−extrusion experiments under high pressure with a thorough investigation on the influence of the

Received: October 24, 2013
Revised: December 18, 2013
Published: January 31, 2014

   dx.doi.org/10.1021/jp4105163 | J. Phys. Chem. C 2014, 118, 3935−3941

intrusion-extrusion steps on the structural and physicochemical properties of the zeosil.

2. EXPERIMENTAL SECTION

2.1. Synthesis of Silicalite-1 Zeolite (MFI-Structure Type). Silicalite-1 was prepared in fluoride medium. This route allows the synthesis of material having a strong hydrophobic character. The synthesis requires the presence of tetrapropylammonium (TPA) cations as structure-directing agents (TPABr, Fluka, purum). Aerosil 130 (Degussa) was used as the silica source. The reaction gel had the following molar composition: 1 SiO_2:0.1 TPABr:0.1 NH_4F:20 H_2O. The mixture, transferred into PTFE-lined stainless-steel autoclaves, was heated at 100 °C for 7 days. After synthesis, the solid was calcined at 550 °C during 6 h in order to remove the organic template.

2.2. Intrusion−Extrusion Experiments. The intrusion−extrusion experiments of aqueous solution in the zeosil sample in the form of compressed and preliminary degassed pellets were performed at room temperature using a modified mercury porosimeter (Micromeritics Model Autopore IV), as described in our previous works.[6] The liquid phase was either pure water or aqueous solution of lithium chloride at different concentrations such as 5, 10, or 20 M. The experimental intrusion−extrusion curves were obtained after subtraction of the curve corresponding to the compressibility of pure water or LiCl aqueous solution. The values of the intrusion (P_{int}) and extrusion (P_{ext}) pressures correspond to that of the half-volume total variation. Pressure is expressed in megapascals (MPa) and volume variation in milliliters (mL) per gram of calcined samples. The experimental error is estimated to 1% on the pressure and on the volume.

After intrusion−extrusion experiments, the samples intruded with LiCl were washed with water to remove traces of LiCl. The absence of chloride anions in the filtrate was checked by adding few drops of 1 M silver nitrate aqueous solution (no silver chloride precipitate). Then the samples were dried at 60 °C overnight and hydrated in a 80% relative humidity atmosphere for 24 h in order to set the hydration state.

2.3. Powder X-ray Diffraction. X-ray diffraction patterns of the different samples were recorded in a Debye−Scherrer geometry on a STOE STADI-P diffractometer equipped with a curved germanium (111), primary monochromator, and a linear position-sensitive detector (6° 2θ) using Cu Kα_1 radiation (λ = 0.15406 nm). Measurements were achieved for 2θ angle values in the 5−50 range, step 0.04° 2θ, and time/step = 40 s. The unit cell parameters were determined using Louër's DICVOL91 indexing routine[22] of the STOE WinXPOW program package.[23]

2.4. Scanning Electron Microscopy. The size and the morphology of the crystals were determined by scanning electron microscopy (SEM) using a Philips XL 30 FEG microscope.

2.5. Nitrogen Adsorption−Desorption Measurements. Nitrogen adsorption−desorption isotherms were performed at −196 °C using a Micromeritics ASAP 2420 apparatus. Prior to the adsorption measurements, the nonintruded samples were outgassed at 300 °C overnight under vacuum. The intruded−extruded samples were outgassed at 90 °C overnight to eliminate physisorbed water and to avoid the dehydroxylation process. The specific surface area (S_{BET}) and microporous volume (V_{micro}) were calculated using the BET and t-plot methods, respectively.

2.6. Thermal Analysis. Thermogravimetric (TG) analyses were carried out on a Setaram TG-Labsys apparatus, under air flow, with a heating rate of 5 °C/min from 20 to 750 °C.

2.7. Solid-State NMR Spectroscopy. ^{1}H MAS, ^{29}Si MAS, and ^{1}H−^{29}Si CPMAS NMR spectra were recorded at room temperature on a Bruker Advance II 300 MHz spectrometer, with a double-channel 7 mm Bruker MAS probe. The recording conditions are given in Table 1.

Table 1. Recording Conditions of the ^{1}H MAS, ^{29}Si MAS, and ^{1}H−^{29}Si CPMAS NMR Spectra

	^{1}H	^{29}Si	
	MAS	MAS	CP MAS
chemical shift standard	TMS[a]	TMS[a]	TMS[a]
frequency (MHz)	300.07	59.6	59.6
pulse width (μs)	5.06	1.87	4
flip angle	$\pi/2$	$\pi/6$	$\pi/2$
contact time (ms)	–	–	1
recycle time (s)	10[b]	80	10[b]
spinning rate (kHz)	4	4	4
scans number	4	1070	8000

[a]TMS: tetramethylsilane. [b]The relaxation time t_1 was optimized.

2.8. ICP/OES Analysis. Measurements by Inductively Coupled Plasma Optical Emission Spectroscopy (ICP-OES) were carried out using a Thermo, Model 6300DUO spectrometer. The lithium concentration was determined after digestion of samples in HF, neutralization by H_3BO_3, filtration and dilution up to 50 mL with ultrapure water. The wavelength of the corresponding spectrometric lines that were used for the analysis was Li: 670.784 nm.

3. RESULTS AND DISCUSSION

3.1. Intrusion−Extrusion Isotherms: Pressure−Volume Diagrams. The pressure−volume diagrams of the "Silicalite-1−water" and the "Silicalite-1−LiCl aqueous solutions" systems are illustrated in Figure 1 and the corresponding characteristic data

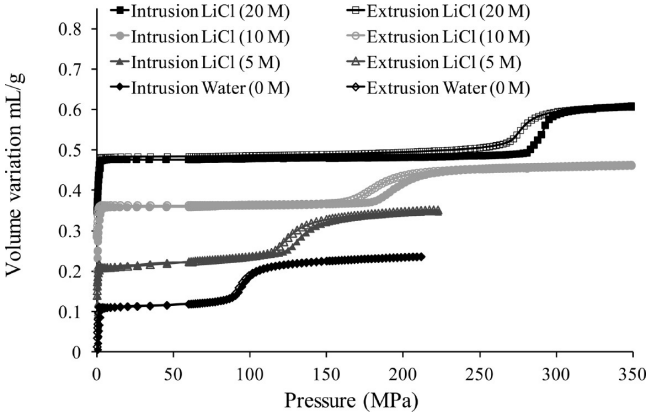

Figure 1. The third intrusion-extrusion cycle of the "Silicalite-1−water" and the different "Silicalite-1−LiCl aqueous solution" systems. For a better visibility, the diagrams are shifted along the *Y*-axis.

are reported in Table 2. For each system, three intrusion-extrusion cycles were performed and the same results were obtained. For clarity only the third intrusion-extrusion cycles are reported in Figure 1. At low pressure (<0.1 MPa), as it was shown in previous works, the volume variation corresponds to the compression and the liquid filling in the interparticular porosity of the zeolitic pellet.[11,13] Beyond this pressure (0.1 MPa), a steep step occurs at a higher pressure. Whatever the system, when the

dx.doi.org/10.1021/jp4105163 | J. Phys. Chem. C 2014, 118, 3935−3941

Table 2. Characteristics of the Samples: Intrusion (P_{int}) and Extrusion (P_{ext}) Pressures, Intruded (V_{int}) and Extruded (V_{ext}) Volumes, and Stored (E_s) and Restored (E_r) Energies

system	P_{int} [a] (MPa)	V_{int} [a] (mL/g)	P_{ext} [a] (MPa)	V_{ext} [a] (mL/g)	E_s [b] (J/g)	E_r [c] (J/g)	energy yield [d] (%)
Silicalite-1−water (0 M)	96	0.10	95	0.10	9.6	9.5	99
Silicalite-1−LiCl (5 M)	133	0.10	128	0.10	13.3	12.8	96
Silicalite-1−LiCl (10 M)	193	0.10	179	0.10	19.3	17.9	93
Silicalite-1−LiCl (20 M)	285	0.11	273	0.10	31.3	27.3	87

[a]Determined from intrusion−extrusion isotherms. [b]Stored energy $E_s = V_{int} \times P_{int}$. [c]Restored energy $E_r = V_{ext} \times P_{ext}$. [d]Percent restored energy = $E_r/E_s \times 100$.

pressure is released down to 0.1 MPa all the liquid is expelled from the porosity of the material meaning that the intrusion−extrusion process is completely reversible. Nevertheless, if a perfect spring behavior is observed for the "Silicalite-1−water" system, the intrusion and extrusion curves being completely superimposable, for the "Silicalite-1−LiCl aqueous solution" systems, a slight hysteresis is observed; the latter increasing with the salt concentration. Therefore, the perfect spring behavior gradually moves slightly toward a shock-absorber behavior. As it will be seen below (TG and NMR sections), this hysteresis might reveal the presence of defect sites (silanol groups) created during the intrusion-extrusion steps. Indeed, these silanol groups interacting with water molecules, an increase of their number leads to longer extrusion step and, thus a larger hysteresis.

The main information on these pressure-volume diagrams is the considerable increase of the intrusion and extrusion pressures with the LiCl concentration. The pressure increases from 96 MPa (pure water) to 285 MPa for LiCl 20 M. This can be explained by a higher solid−liquid interfacial tension. Another way to explain the pressure increase could be the ions desolvation phenomenon[19] or the size of solvated ions.[20,21] Indeed, in the LiCl solutions each lithium ion is solvated by a number of water molecules which depends on the LiCl concentration, consequently, the intrusion pressure could be influenced by this parameter.

For the "Silicalite-1−water", the intruded volume, close to 0.10 mL/g, is lower than the one obtained from N_2 adsorption−desorption isotherms (see below, i.e., 0.17 mL/g). Such a difference was explained by Desbiens et al. by a lower density of water in the MFI structure (0.6 instead of 1g/mL).[5] For the "Silicalite-1−LiCl aqueous solution" systems, a similar intruded volume is obtained (see Table 2, i.e., 0.10 to 0.11 mL/g).

Compared to the "Silicalite-1−water" system (yield = 99%; stored energy ≈ 10 J/g), the "Silicalite-1−LiCl aqueous solution" systems restore 96, 93, or 87% of the stored energy corresponding to about 13, 19, or 31 J/g, respectively (Table 2). Therefore, in the case of the LiCl 20 M, the energetic performances are tripled.

3.2. XRD and SEM Characterizations. The XRD patterns of the calcined samples before and after intrusion−extrusion experiments reported in Figure 2 are very similar, which means that at the long-range order, the MFI structure is not affected. They can be indexed in the monoclinic symmetry (space group $P2_1/n$). The corresponding unit cell parameters are reported in Table 3.

A slight increase of the unit cell volume (from 5349 to 5379 Å^3) is observed when the LiCl concentration increases. The creation of defect sites might be responsible of this change.

The crystal morphology of Silicalite-1 was examined by scanning electron microscopy. For the nonintruded Silicalite-1 sample, twinned coffin shaped crystals with sizes close to 17 × 8 × 3 μm^3 are observed (Figure 3a). After the intrusion−extrusion experiments, most of the crystals are broken (Figure 3b−e).

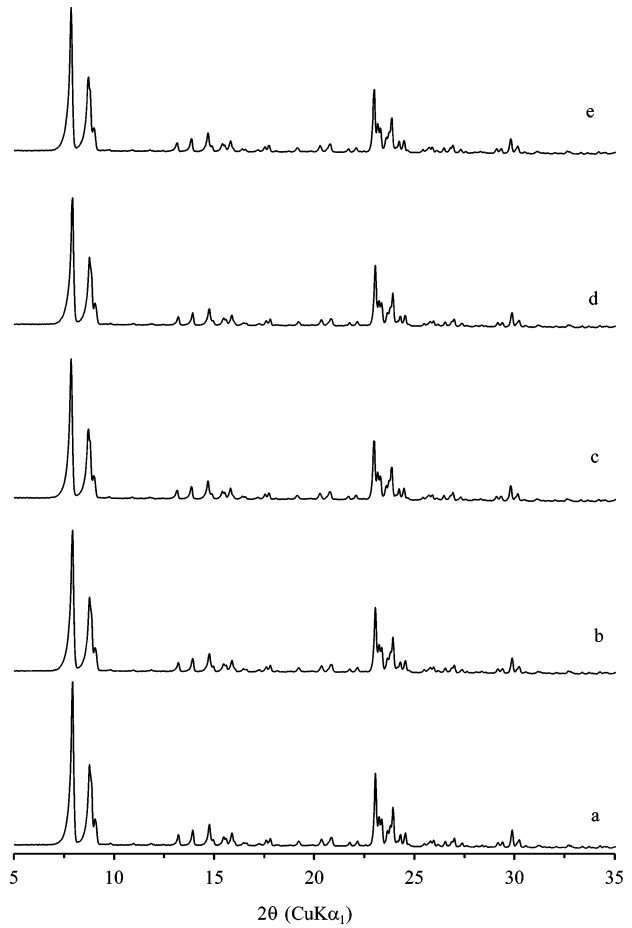

Figure 2. X-ray diffraction patterns of calcined Silicalite-1 samples before (a) and after three intrusion−extrusion cycles in (b) water, (c) LiCl 5 M, (d) LiCl 10 M, and (e) LiCl 20 M.

3.3. N_2 Adsorption−Desorption Isotherms. The N_2 adsorption−desorption isotherms of the nonintruded and intruded samples are shown in Figure 4. In all cases, the isotherms are mainly of type I characteristic of microporous solids with the presence of a clear step for relative pressures slightly above 0.15, followed by a plateau. As has been described by Llewellyn et al.[24] this step corresponds to a density change of the adsorbed phase. It was ascribed to a phase transition from a lattice fluid-like phase to a crystalline-like solid phase. The BET surface area and microporous volume of samples are quite similar and equal to 373 m^2/g and 0.17 cm^3/g, respectively for the nonintruded sample and intruded-extruded ones with LiCl 0 M, 5 and 10 M. For the intruded-extruded sample with LiCl 20 M, these data slightly decrease (S_{BET} = 350 m^2/g and V_{micro} = 0.16

dx.doi.org/10.1021/jp4105163 | J. Phys. Chem. C 2014, 118, 3935−3941

Table 3. Unit Cell Parameters of Calcined Silicalite-1 Samples before and after Three Intrusion−Extrusion Cycles in Water, LiCl 5 M, LiCl 10 M, and LiCl 20 M

sample	a (Å)	b (Å)	c (Å)	β (deg)	V (Å^3)
nonintruded sample	19.887(10)	20.115(9)	13.373(6)	90.66(4)	5349.2(58)
intruded−extruded sample (in pure water, 0 M)	19.880(8)	20.113(7)	13.379(6)	90.63(3)	5349.4(52)
intruded−extruded sample (in LiCl, 5 M)	19.908(10)	20.131(9)	13.371(7)	90.64(4)	5358.5(59)
intruded−extruded sample (in LiCl, 10 M)	19.897(8)	20.118(7)	13.378(6)	90.58(3)	5354.7(48)
intruded−extruded sample (in LiCl, 20 M)	19.949(8)	20.148(9)	13.385(7)	90.60(4)	5379.8(56)

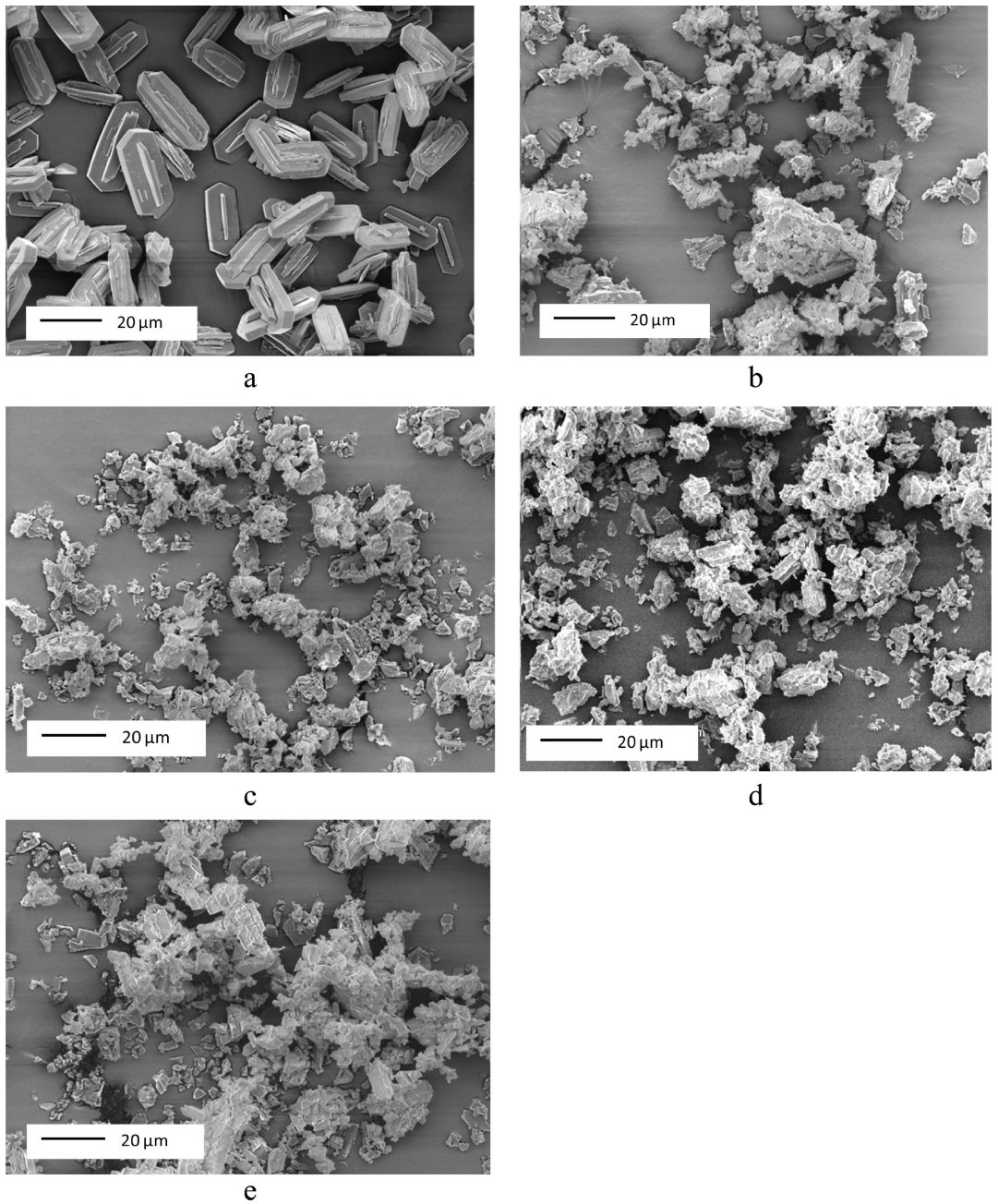

Figure 3. SEM micrographs of the calcined Silicalite-1 samples before (a) and after three intrusion-extrusion cycles in (b) water, (c) LiCl 5 M, (d) LiCl 10 M, and (e) LiCl 20 M.

cm^3/g) revealing thus the creation of few defect sites in this sample.

3.4. Thermal Analysis. The experimental results issued from the thermogravimetric (TG) analysis of the Silicalite-1 samples before and after intrusion-extrusion experiments are depicted in Figure 5. In all cases, the total weight loss is quite low, ranging from 0.48 to 1.79 w % and increases with the electrolyte concentration. The weight losses occur in two steps. The first one (0.22 to 1.24 wt %), located between 20 and 200 °C, is ascribed to the desorption of the physisorbed water molecules. The

dx.doi.org/10.1021/jp4105163 | J. Phys. Chem. C 2014, 118, 3935−3941

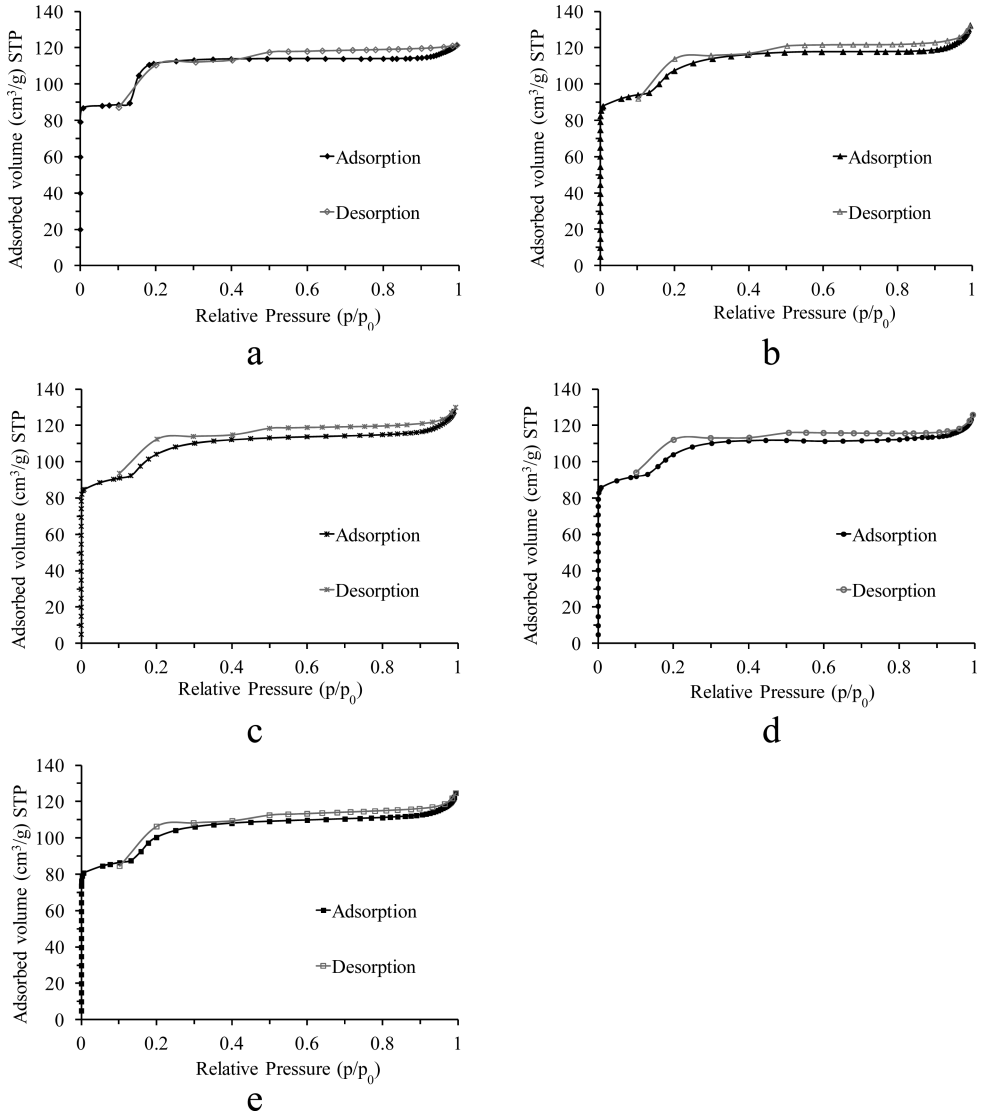

Figure 4. N_2 adsorption−desorption isotherms at −196 °C of the calcined Silicalite-1 sample before (a) and after three intrusion-extrusion cycles in (b) water, (c) LiCl 5 M, (d) LiCl 10 M, and (e) LiCl 20 M.

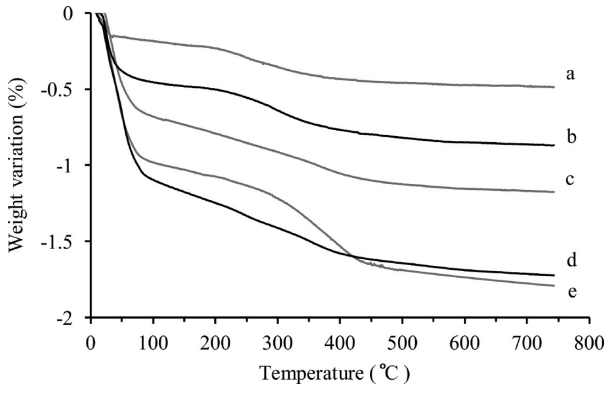

Figure 5. TG curves of the calcined Silicalite-1 samples before (a) and after three intrusion-extrusion cycles in (b) water, (c) LiCl 5 M, (d) LiCl 10 M, and (e) LiCl 20 M.

second weight loss, in the temperature range 200−600 °C, can be assigned to water arising from dehydroxylation reactions leading to 1.7 and 5 OH groups per unit cell for the nonintruded sample and the intruded-extruded one with LiCl 20 M, respectively. From these TG curves, it appears clearly that the silanol groups increase with the LiCl concentration. These silanol groups result from the breaking of siloxane bonds and are probably created due to the high pressure involved during the intrusion-extrusion experiments. The whole of these results will be confirmed by ^{29}Si solid-state NMR.

3.5. ^{29}Si MAS, ^{1}H−^{29}Si CPMAS, and ^{1}H-MAS NMR Spectroscopy. *3.5.1. ^{29}Si MAS NMR Spectroscopy.* The ^{29}Si MAS NMR spectra of the calcined MFI-type zeosil before and after intrusion−extrusion experiments are shown in Figure 6. The spectrum of the starting Silicalite-1 material (Figure 6a) exhibit 8 resonances in the −108 to 118 ppm range ascribed to the 24 non equivalent crystallographic silicon sites, no signals assigned to Q_3 groups corresponding to defects such as Si−OH groups and expected at about −100 ppm are observed. After the intrusion−extrusion steps in LiCl aqueous solution (0, 5, 10, and 20 M) (Figure 6b−e), all spectra are completely superimposable, indicating no significant modification of the local structural order in the inorganic framework (the detection limit is around 5% of Si sites which corresponds to about 5 OH per unit cell).

dx.doi.org/10.1021/jp4105163 | J. Phys. Chem. C 2014, 118, 3935−3941

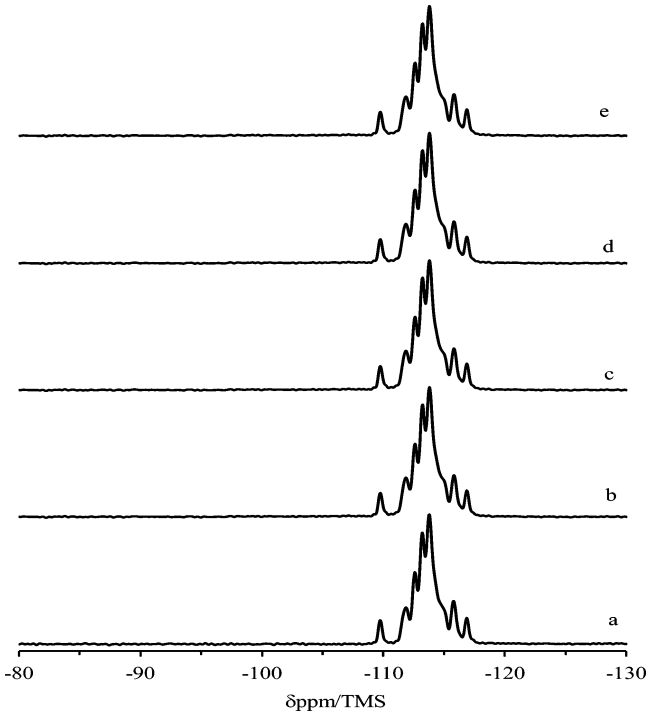

Figure 6. ^{29}Si MAS NMR spectra of the calcined Silicalite-1 sample before (a) and after three intrusion−extrusion cycles in (b) water, (c) LiCl 5 M, (d) LiCl 10 M, and (e) LiCl 20 M.

3.5.2. ^{1}H−^{29}Si CPMAS NMR Spectroscopy. The ^{1}H−^{29}Si CPMAS NMR spectra of the calcined nonintruded and intruded samples are reported in Figure 7. These spectra were performed

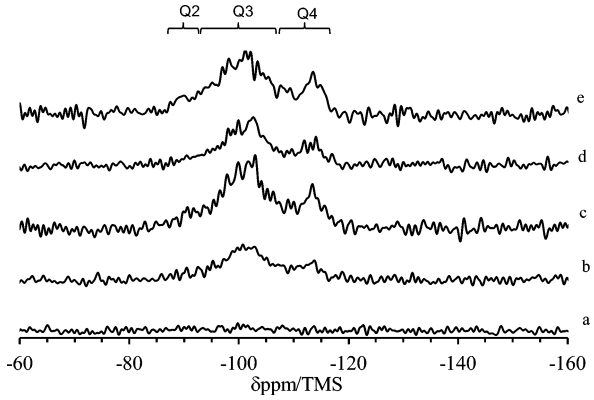

Figure 7. ^{1}H−^{29}Si CPMAS NMR spectra of the calcined Silicalite-1 sample before (a) and after three intrusion-extrusion cycles in (b) water, (c) LiCl 5 M, (d) LiCl 10 M, and (e) LiCl 20 M.

in order to enhance the silicon atoms that bear protons and thus to get evidence of the presence of silanol groups. As expected, under these NMR experimental conditions (very short contact time), the spectrum of the nonintruded Silicalite-1 sample provides a barely visible signal (Figure 7a) indicating that no or only very few defect sites are present (the detection limit is 2% of Si sites; about 2 OH per unit cell). After intrusion−extrusion experiments, the presence of two resonances are clearly detected at around −90 and −100 ppm (Figure 7b−e) corresponding to the Q_2 ($(HO-)_2Si(-OSi)_2$) and Q_3 ($HO-Si(-OSi)_3$) groups, respectively. These spectra (with high scans number) display a low signal-to-noise ratio which means that the number of silanol groups is very low, confirming thus what is observed above by ^{29}Si MAS NMR spectroscopy. ^{1}H−^{29}Si CPMAS NMR experiments are not quantitative, and deconvolution can be hazardous. Nevertheless, compared to the intruded-extruded sample with water (0 M) the relative number of Q_2 + Q_3 species increases from 80 to 85% for the intruded-extruded sample with LiCl (20 M), indicating that the number of defects increase.

3.5.3. ^{1}H-MAS NMR. The ^{1}H-MAS NMR spectra of the calcined nonintruded and intruded samples are reported in Figure 8. Among all studied "Silicalite-1−LiCl aqueous solution"

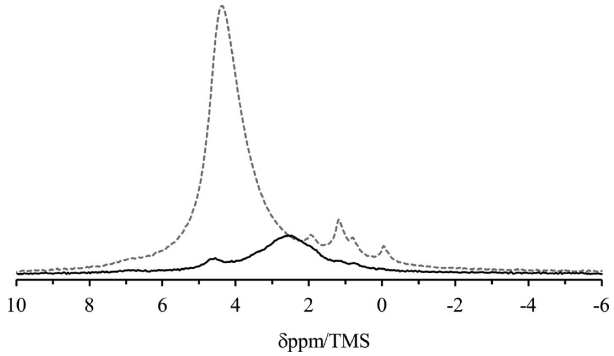

Figure 8. ^{1}H−MAS NMR spectra of the calcined Silicalite-1 sample before (thick solid line) and after three intrusion−extrusion cycles in LiCl 20 M (dotted line).

systems, only the ^{1}H-MAS NMR of the "Silicalite-1−LiCl 20 M" system is presented in this paper. Indeed, as demonstrated by TG analysis, the highest rate of silanol groups is observed for this LiCl concentration. The ^{1}H-MAS NMR technique is an efficient tool to characterize the hydrogenated species in silicates. In agreement with the results discussed above, the signal recorded for the calcined nonintruded sample is very low (Figure 8, thick solid line), indicating that the defect sites are few and that this sample is mainly hydrophobic. The spectrum of the intruded-extruded Silicalite-1 sample with LiCl 20 M (Figure 8, dotted line) reveals a main component at 4.3 ppm characteristic of water molecules[25] and three resonances at 0.8, 1.15, and 2 ppm corresponding to silanol groups (≡Si−OH).[25] The appearance of a new resonance is observed at −0.1 ppm. Such a component was previously observed in the water intruded-extruded CHA-type zeosil[8] and assigned to neighboring silanols obtained after one siloxane Si−O−Si bond break or to a unique water molecule in a hydrophobic environment. From the comparison of both spectra and as seen above by TG analysis, it appears clearly that the number of silanol groups and water molecules is larger in the intruded extruded samples with LiCl 20 M.

3.6. ICP/OES Analysis. In order to get or not evidence of the presence of lithium ions, after intrusion−extrusion experiments, ICP/OES analysis was performed. The intruded-extruded sample with LiCl 20 M contains about 0.1 wt % of lithium, corresponding to about one lithium atom per unit cell (96 Si). This content is too low to be assigned. It might correspond to lithium in interaction with Q_3 group of type $^{-}O-Si(-OSi)_3$.

4. CONCLUSION

This work highlights the influence of LiCl aqueous solution concentration on the energetic performances of Silicalite-1 zeolite under high intrusion pressure. Compared to the perfect spring behavior observed for the "Silicalite-1−water" system, the "Silicalite-1−LiCl aqueous solution" systems move toward a

dx.doi.org/10.1021/jp4105163 | J. Phys. Chem. C 2014, 118, 3935−3941

shock-absorber behavior which grows up with the increase of salt concentration. For these latter systems all the liquid is expelled from the solid when the pressure reaches to 0.1 MPa. However, the intrusion pressure increases with the concentration of the electrolyte from 96 MPa for pure water up to 285 MPa for LiCl 20 M. Therefore, compared to the "Silicalite-1−water" system, the stored energy is tripled for the "Silicalite-1−LiCl 20 M" system.

After the intrusion−extrusion experiments, slight defects are observed in the MFI structure. The breaking of some siloxane bridges was clearly revealed by the presence of Q_2 and Q_3 groups on the $^{1}H-^{29}Si$ CPMAS NMR spectra and the creation of the resulting hydroxyl groups quantified by TG experiments. These defects are probably responsible for the hysteresis observed on the intrusion-extrusion curves of the "Silicalite-1−LiCl aqueous solution" systems.

AUTHOR INFORMATION

Corresponding Authors

*E-mail: (T.J.D.) jean.daou@uha.fr. Telephone: ++33 (0)3 89 33 67 39. Fax: ++33 (0)3 89 33 68 85.
*E-mail: (J.P.) joël.patarin@uha.fr. Telephone: ++33 (0)3 89 33 68 80. Fax: ++33 (0)3 89 33 68 85.

Notes

The authors declare no competing financial interest.

REFERENCES

(1) Čejka, J.; Van Bekkum, H.; Corma, A.; Schüth, F. Introduction to Zeolite Science and Practice. *Stud. Surf. Sci. Catal.* **2007**, *168*, 525−544.
(2) Lewis, N. S. Toward Cost-Effective Solar Energy Use. *Science* **2007**, *315*, 798−801.
(3) Eroshenko, V.; Regis, R. C.; Soulard, M.; Patarin, J. Energetics: A New Field of Applications for Hydrophobic Zeolites. *J. Am. Chem. Soc.* **2001**, *123*, 8129−8130.
(4) Saada, M.-A.; Soulard, M.; Marler, B.; Gies, H.; Patarin, J. Pressure Water Intrusion Investigation of Pure Silica RUB-41 and S-SOD Zeolite Materials. *J. Phys. Chem. C* **2011**, *115*, 425−430.
(5) Desbiens, N.; Demachy, I.; Fuchs, A.; Kirsh-Rodeschini, H.; Soulard, M.; Patarin, J. Water Condensation in Hydrophobic Nanopores. *Angew. Chem., Int. Ed.* **2005**, *44*, 5310−5313.
(6) Trzpit, M.; Soulard, M.; Patarin, J. The pure silica chabazite: A High Volume Molecular Spring at Low Pressure for Energy Storage. *Chem. Lett.* **2007**, *36*, 980−981.
(7) Trzpit, M.; Soulard, M.; Patarin, J.; Desbiens, N.; Cailliez, F.; Boutin, A.; Demachy, I.; Fuchs, A. The Effect of Local Defects on Water Adsorption in Silicalite-1 Zeolite: A Joint Experimental and Molecular Simulation Study. *Langmuir* **2007**, *23*, 10131−10139.
(8) Trzpit, M.; Rigolet, S.; Paillaud, J.-L.; Marichal, C.; Soulard, M.; Patarin, J. Pure Silica Chabazite Molecular Spring: A Structural Study on Water Intrusion−Extrusion Processes. *J. Phys. Chem. B* **2008**, *112*, 7257−7266.
(9) Tzanis, L.; Trzpit, M.; Soulard, M.; Patarin, J. High Pressure Water Intrusion Investigation of Pure Silica 1D Channel AFI, MTW and TON-Type Zeolites. *Microporous Mesoporous Mater.* **2011**, *146*, 119−126.
(10) Tzanis, L.; Trzpit, M.; Soulard, M.; Patarin, J. Energetic Performances of Channel and Cage-Type Zeosils. *J. Phys. Chem. C* **2012**, *116*, 20389−20395.
(11) Tzanis, L.; Marler, B.; Gies, H.; Soulard, M.; Patarin, J. High-Pressure Water Intrusion Investigation of Pure Silica ITQ-7 Zeolite. *J. Phys. Chem. C* **2013**, *117*, 4098−4103.
(12) Bushuev, Y. G.; Sastre, G. Atomistic Simulation of Water Intrusion-Extrusion in ITQ-4 (IFR) and ZSM-22 (TON): The Role of Silanol Defects. *J. Phys. Chem. C* **2011**, *115*, 21942−24953.
(13) Ortiz, G.; Nouali, H.; Marichal-Westrich, C.; Chaplais, G.; Patarin, J. Energetic Performances of the Metal−Organic Framework ZIF-8 Obtained Using High Pressure Water Intrusion−Extrusion Experiments. *Phys. Chem. Chem. Phys.* **2013**, *15*, 4888−4891.
(14) Martin, T.; Lefevre, B.; Brunel, D.; Galarneau, A .; Di Renzo, F .; Fajula, F.; Gobin, P. F.; Quinson, J. F.; Vigier, G. Dissipative Water Intrusion in Hydrophobic MCM-41 Type Materials. *Chem. Commun.* **2002**, 24−25.
(15) Guillemot, L.; Galarneau, A.; Vigier, G.; Abensur, T.; Charlaix, É. New Device to Measure Dynamic Intrusion/Extrusion Cycles of Lyophobic Heterogeneous Systems. *Rev. Sci. Instrum.* **2012**, *83*, 105−107.
(16) Lefevre, B.; Saugey, A.; Barrat, J. L.; Charlaix, E.; Gobin, P. F.; Vigier, G. Intrusion and Extrusion of Water in Highly Hydrophobic Mesoporous Materials: Effect of the Pore Structure. *Colloids Surf. A: Physicochem. Eng. Aspects* **2004**, *241*, 265−272.
(17) Lefevre, B.; Saugey, A.; Barrat, J. L.; Bocquet, J. L.; Charlaix, E.; Gobin, P. F.; Vigier, G. Intrusion and Extrusion of Water in Hydrophobic Mesopores. *J. Chem. Phys.* **2004**, *120*, 4927−4938.
(18) Han, A.; Lu, W.; Kim, T.; Chen, X.; Qiao, Y. Influence of Anions on Liquid Infiltration and Defiltration in a Zeolite Y. *Phys. Rev. E* **2008**, *78*, 031408−031411.
(19) Tzanis, L.; Nouali, H.; Daou, T. J.; Soulard, M.; Patarin, J. Influence of the Aqueous Medium on the Energetic Performances of Silicalite-1. *Mater. Lett.* **2014**, *115*, 229−232.
(20) Han, A.; Punyamurtula, V K.; Qiao, Y. Effects of Cation Size on Infiltration and Defiltration Pressures of a MCM-41. *Appl. Phys. Lett.* **2008**, *92*, 153117.
(21) Liu, L.; Chen, X.; Kim, T.; Han, A.; Qiao, Y. Effects of Anion Size and Concentration on Electrolyte Invasion into Molecular-Sized Nanopores. *New J. Phys.* **2010**, *12*, 033021.
(22) Boultif, A.; Louër, D. Indexing of Powder Diffraction Patterns for Low-Symmetry Lattices by the Successive Dichotomy Method. *J. Appl. Crystallogr.* **1991**, *24*, 987−993.
(23) *STOE WinXPOW*, version 1.06; STOE and Cie: Darmstadt, Germany, 1999.
(24) Llewellyn, P. L.; Coulomb, J. P.; Grillet, Y.; Patarin, J.; Andre, G.; Rouquerol, J. Adsorption by MFI-Type Zeolites Examined by Isothermal Microcalorimetry and Neutron Diffraction. 2. Nitrogen and Carbon Monoxide. *Langmuir* **1993**, *9*, 1852−1856.
(25) Burneau, A.; Gallas, J. P. In *The Surface Properties of Silicas*; Legrand, A. P., Ed.; John Wiley & Sons: Chichester, U.K., 1998; pp 145−234.